Geophysical Research Letters

RESEARCH LETTER
10.1029/2021GL097580

Extreme Exospheric Dynamics at Charon: Implications for the Red Spot

Ben Teolis[1,2,3], Ujjwal Raut[1,2,3], Joshua A. Kammer[2], Caleb J. Gimar[1,2,3], Carly J. A. Howett[4], G. Randall Gladstone[2,3], and Kurt D. Retherford[1,2,3]

[1]Center for Laboratory Astrophysics and Space Science Experiments (CLASSE), Space Science and Engineering, Southwest Research Institute, San Antonio, TX, USA, [2]Space Science and Engineering, Southwest Research Institute, San Antonio, TX, USA, [3]Department of Physics and Astronomy, University of Texas at San Antonio, San Antonio, TX, USA, [4]Department of Space Studies, Southwest Research Institute, Boulder, CO, USA

Key Points:

- Surges in Charon's exosphere, driven by spring-sunrise sublimation of polar methane, produce "flash frozen" CH_4 frost at the autumn pole
- Polar frost grows too thick and fast for efficient Ly-α CH_4 photolysis to hydrocarbons past C_2H_6 that may contribute to Charon's red spot
- Origin of Charon's polar red material may be in part solar wind radiolysis of photolytic ethane remaining surface-bound past spring sunrise

Supporting Information:

Supporting Information may be found in the online version of this article.

Correspondence to:

B. Teolis,
ben.teolis@swri.org

Citation:

Teolis, B., Raut, U., Kammer, J. A., Gimar, C. J., Howett, C. J. A., Gladstone, G. R., & Retherford, K. D. (2022). Extreme exospheric dynamics at Charon: Implications for the red spot. *Geophysical Research Letters*, *49*, e2021GL097580. https://doi.org/10.1029/2021GL097580

Received 17 JAN 2022
Accepted 2 APR 2022

The copyright line for this article was changed on 28 JUN 2022 after original online publication.

Abstract Charon's exosphere may exhibit extreme seasonal dynamics, with centuries of quiescence punctuated by short lived (~4 earth years) exospheric surges near the equinoxes, as spring sunrise bi-annually drives frozen methane off the polar night zones. Charon's pole-centric red spot has been proposed to be the product of Ly-α photolysis of frozen methane into refractory hydrocarbon "tholins", but the role of exospheric dynamics in the red material's formation has not been investigated. We show with exospheric modeling that methane "polar-swap", in which exospheric CH_4 sublimated from the spring polar zone is rapidly re-frozen onto the autumn hemisphere, deposits ~30 μm polar frosts too thick for Ly-α light to penetrate. Ethane, the primary methane photoproduct under these conditions, may unlike methane remain frozen decades after polar sunrise under solar wind exposure. Solar wind radiolysis of polar ethane frost synthesizes higher-order refractories that may contribute to the coloration of Charon's polar zones.

Plain Language Summary Charon's thin methane atmosphere undergoes "explosive" pulsations owing to the Pluto-Charon's systems' near sideways tilt to the Sun, according to new computer simulations that we present here. Spring sunrise may drive polar methane frozen during the centuries long winter night back into Charon's atmosphere, causing the whole atmosphere to briefly and drastically surge in pressure by a factor of almost 1000 every equinox. During these exceedingly brief episodes, taking place just a few years out of the Pluto-Charon system's 248 year orbit around the Sun, polar caps of methane frost tens of microns thick may be suddenly swapped between north and south, evaporated and then re-frozen from the spring to the autumnal polar zones. Charon's polar red spot, seen by the New Horizons spacecraft, is suspected to be material synthesized from frozen methane by backscattered solar ultraviolet light. However we find that Charon's polar caps are frozen too fast and thick for synthesis of much material more complex than ethane. Nevertheless ethane, being less volatile than methane, stays frozen to Charon's surface for decades after spring sunrise, and may under exposure to solar wind be converted to permanent red-colored surface deposits that contribute to the origins of the red spot.

1. Introduction

Charon's reddish "Mordor Macula" polar terrain, imaged by the New Horizons MVIC instrument (Reuter et al., 2008) in 2015, may be the most visible example of atmospheric cold trapping in the solar system. The red material, centered around the north polar zone (Figure 1), and similar albedo-dark terrain seen in lower resolution LORRI (Cheng et al., 2008) imaging of the south, are proposed (Grundy et al., 2016) to be surface refractory hydrocarbon "tholins" formed from UV photolysis of methane frost cold trapped out of a Charon CH_4 exosphere. Exospheric methane condensed onto Charon's polar night zones is constantly exposed to solar Ly-α photons backscattered by interplanetary hydrogen (Gladstone et al., 2015). Although Charon's exosphere was too tenuous for detection at the time of the New Horizons encounter (Stern et al., 2017), models show (Hoey et al., 2017; Tucker et al., 2015) that some methane molecules escaping Pluto's atmosphere are gravitationally focused and impacted/captured by Charon along its orbit.

However, extreme seasons influence Charon's surface temperature and exosphere owing to the Charon-Pluto system's high 119° axial tilt. Spring sunrise surface heating drives frozen methane off the polar zones, leading to bi-annual cycles of freezing and sublimation of methane to/from the polar terrains, and a highly seasonal methane

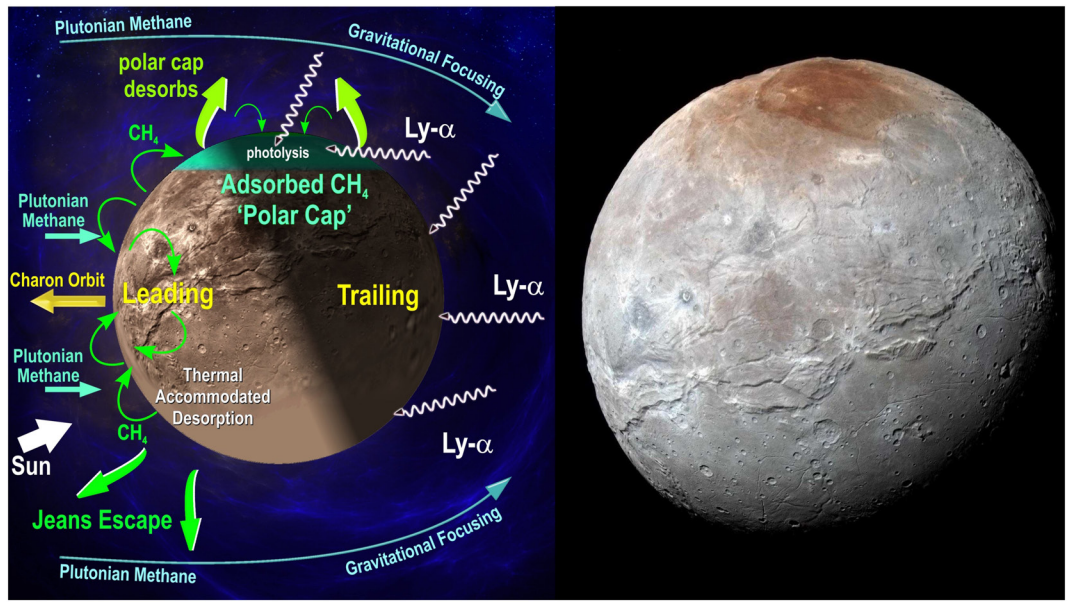

Figure 1. Left: Several key physical processes occurring at Charon considered in our exospheric modeling, including CH_4 arrival onto the leading hemisphere, CH_4 propagation and adsorption in the winter polar region, CH_4 photo-conversion, and escape. Right: MVIC enhanced color image of Charon using MVIC's Near IR, Red and Blue filters for RGB color (PIA19968). Charon's red Mordor Macula terrain spreads across its north pole, shown here toward the top of the image.

exosphere. In such a dynamic Charon exosphere, bound by gravity, we must augment the original idea (Grundy et al., 2016) of methane arriving from Pluto steadily condensing onto the polar night zone, to now include the possibility of polar CH_4 freezing to the night zone in seasonal surges. In this paper, we model Charon's seasonal exosphere to understand the role of extreme exospheric dynamics in determining the distribution and extent of methane, and of red material around the poles.

2. Exospheric Modeling

Charon's exospheric physics are illustrated in Figure 1. An estimated $\sim 6 \times 10^{11}$ m^{-2} s^{-1} methane ram flux from Pluto impacts Charon's leading hemisphere (Hoey et al., 2017). Methane impacting Charon thermally accommodates to the ~10–60 K surface temperature (Figure S1 in Supporting Information S1), leaving most (~99% at 60 K) CH_4 molecules with insufficient energy to overcome Charon's 590 m/s escape speed. The resulting gravitationally bound exosphere has according to our modeling densities of $\sim 10^9$–10^{14} CH_4/m^3 at the surface. At these low densities the exosphere is essentially collisionless. Methane molecules execute uninterrupted "hops" across the surface (we estimate an average 25 min time of flight per hop) until they either (a) gravitationally escape (with an ~1% probability per hop), or (2) become cold trapped at the poles. Charon's polar winter surface temperatures drop as low as 15(±5) K (Grundy et al., 2016), which can efficiently cold-trap methane out of the exosphere. Solar Ly-α is backscattered by interplanetary H onto the night side, exposing condensed methane to surface photolysis. The fraction of methane converted into higher-order hydrocarbons by Ly-α light depends on (a) the thickness of the methane frost, (b) the optical absorption depth into solid methane, and (c) the relative rates (vs. surface position and time) of methane condensation and photolysis. The remaining un-converted polar frost desorbs back into the exosphere at spring sunrise, producing semi-annual springtime maxima in the density of Charon's entire exosphere. As we discuss, these transient exospheres exist only a few years out of the Pluto-Charon system's entire 248 year heliocentric orbit.

Our Monte Carlo exospheric simulation (Teolis & Waite, 2016) considers: (a) The CH_4 arrival flux onto Charon's leading hemisphere, (b) Charon's rotation and gravity field, (c) diurnal and seasonal methane adsorption/desorption to/from the surface, and (d) Ly-α photolysis of condensed methane into photoproducts. The methane source to Charon is the CH_4 impact flux from Pluto modeled by Hoey et al. (2017) centered on Charon's leading hemisphere apex with an approximate $F_1 \times \cos(\theta) + F_2$ distribution, with $F_1 = 2 \times 10^{11}$ m^{-2} s^{-1}, $F_2 = 5.5 \times 10^{11}$ m^{-2} s^{-1}

and θ the angular distance from the apex. Charon's exospheric dynamics are largely driven by condensation and sublimation of methane already present at Charon (with CH_4 persisting an average ∼155 years, exceeding two seasons), and respond only slowly to (as yet poorly constrained) changes in the source from Pluto. We have therefore considered here a constant CH_4 source to Charon, as any seasonal variability in Pluto's methane escape rate only weakly affects the exosphere's predicted variability. Simulation molecules stick transiently to the surface and desorb stochastically at a rate $C \times \exp(E/kT)$, with $C = 2.9 \times 10^{-14}$ s^{-1} (Armstrong et al., 1955) and binding energy E, ejecting with a Maxwell-Boltzmann velocity distribution at the local surface temperature T and a cosine ejection angular distribution. A binding energy $E \sim 0.11$ eV is implied by the vapor pressure curve of pure methane (Armstrong et al., 1955). However the curve may have some sensitivity to photoproduct concentrations in Charon's methane frost, and we therefore considered in some simulations a small (50%) enhancement of E, similar to the enhanced exospheric O_2 and Ar surface binding at Dione, Rhea (Teolis & Waite, 2016) and the Moon (Grava et al., 2015) and attributed to surface radiation chemical activation. We model the surface temperature using the standard approach applied by Grundy et al. (2016); that is, by (a) taking into consideration the estimated thermal inertia range (2.5–40 J m^{-2} K^{-1} s$^{-1/2}$), albedo (∼0.3) and emissivity (∼0.9) (Grundy et al., 2016), respectively, and the seasonal time evolution of solar insolation versus position, and by (b) solving the thermal diffusion equation versus depth, location (latitude, local time), and time-of-year. The ejected molecules are propagated along uninterrupted trajectories before either escaping Charon's gravity (non-gravitational escape processes such as ion pickup (Bagenal et al., 2016) and photo-dissociation (Huebner et al., 1992) are comparatively negligible), or returning to the surface to stick again. The simulated molecules hop in random walk fashion, redistributing themselves around the satellite to generate uneven and evolving distributions of exospheric gas and surface condensate.

We modeled Ly-α photolysis using the photo-conversion cross section $\sigma_d = 9 \times 10^{-22}$ m^2 (Raut et al., 2022) with the equation $d\eta/dt = F_{CH_4} - \sigma_d F_{Ly\alpha} \eta_0$ for the competition of CH_4 accretion flux F_{CH_4} (net adsorption minus desorption) with conversion to photoproducts by Ly-α photons (with flux $F_{Ly\alpha} = 3.5 \times 10^{11}$ m^{-2}s^{-1} (Grundy et al., 2016)). Here η denotes methane column density frozen to the surface versus time t, while η_0 is the CH_4 column density in range of the Ly-α light: We assume $\eta_0 = \rho d \sim 7 \times 10^{20}$ m^{-2} (methane density times Ly-α absorption depth) if $\eta > \rho d$, and $\eta_0 = \eta$ if $\eta \leq \rho d$. The exospheric simulation numerically evaluates this equation across Charon's surface, destroying the required fraction of the surface-bound methane molecules at every time step. Maps (Figure 4) of the predicted photoproduct production rate by Ly-α photolysis (CH_4/s/m^2 destroyed) versus position and time are a product of the evaluation of this equation by our exospheric model.

3. Results and Discussion

Drastic seasonal oscillations of exospheric density and abundance are predicted by the exospheric model as shown in Figure 2. During the decades-long polar winters a methane "frost cap" of several hundred nanometers thickness gradually accumulates in the polar night zone, and Charon's exospheric density is limited to a low level (∼5×10^{29} CH_4 molecules in the exosphere). Since CH_4 arriving at the leading hemisphere reaches the polar zone within only a few random walk hops, the exosphere does not have a chance to distribute itself evenly before freezing to the surface, and the gas density at Charon's surface is ∼2 times greater over the leading hemisphere than the trailing (∼1 and 0.5×10^{11} CH_4/m^3 surface density, respectively). Only ∼0.01% of the CH_4 molecules are actually in flight in the exosphere during these winter periods, with the remaining 99.99% stuck to Charon's polar night surface.

The approach of vernal equinox drastically changes this situation, as the poleward advance of the solar terminator (Figure S1 in Supporting Information S1) prompts methane sublimation from the edge of the polar night zone. At first most of these methane molecules migrate back into the shrinking polar night zone and refreeze, possibly after executing a few random walk hops around Charon. However, as the polar night zone continues to shrink, this "push broom" effect focuses the methane frost cap to an ever-smaller area around the pole.

Finally, at vernal equinox the polar night zone disappears entirely, and the polar sunrise forces most of the methane frost into the exosphere, prompting a brief but drastic "burst" of gas density over Charon's entire exosphere (Figures 2 and 3). Within roughly four Earth years Charon's exospheric abundance is predicted by the model to surge, and then crash, through ∼3 orders of magnitude as shown in Figure 2. The maximum predicted ∼6×10^{18} CH_4/m^2 vertical column density is far below the ∼3.5×10^{23} CH_4/m^2 upper limit from Earth-based

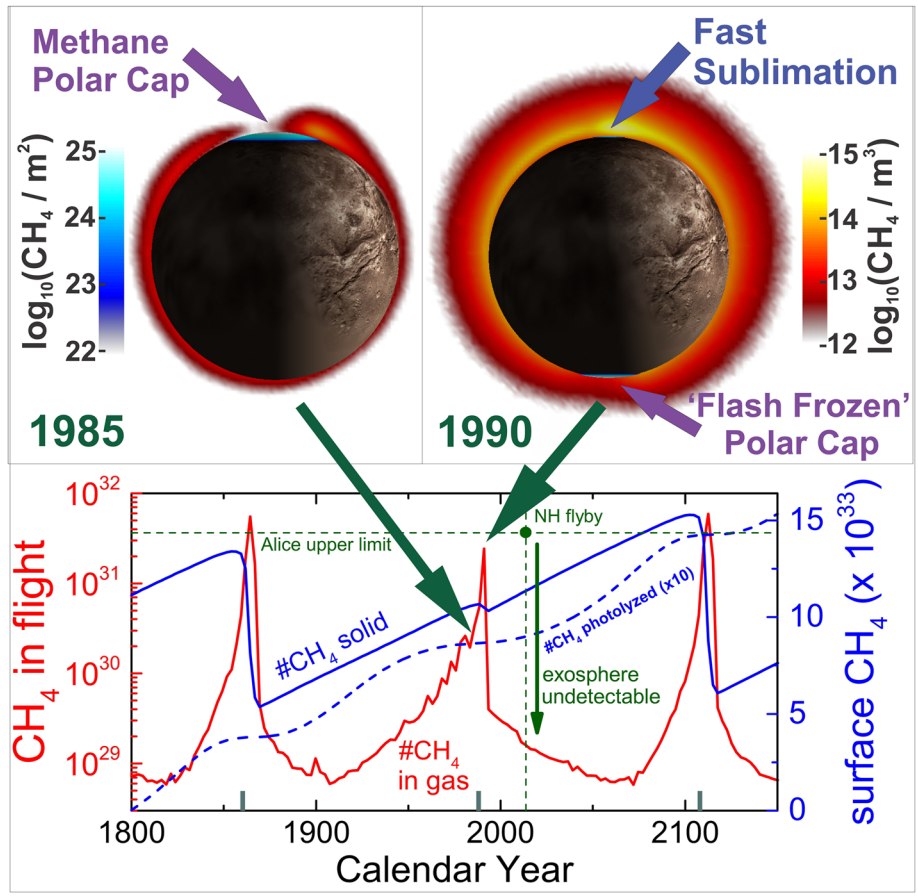

Figure 2. Top: Two snapshots of Charon's evolving exospheric gas (red color: noon-to-midnight CH_4 density cross section, dawn equatorial view) and surface condensate (blue color: CH_4 adsorbed column density) in the years 1985 (left) and 1990 (right), before and after equinox (16 Dec 1987) to show the "ramp up" of exospheric density. Simulation used a 10 m^{-2} K^{-1} $s^{-1/2}$ thermal inertia. Bottom: Total CH_4 molecules in the model exosphere (red) and on the surface (blue solid) versus time (equinoxes: x-axis ticks), and the cumulative number of CH_4 molecules photo-converted to surface photoproducts over one Pluto orbit (blue dashed). The predicted exospheric abundance is well below detectability (Stern et al., 2017) by New Horizons. At the Pluto-Charon systems' present orbital perihelion longitude, the modeled methane polar caps are being flash frozen in the south but slowly accreted in the north. Accordingly, the frozen CH_4 abundance drops less drastically near the 1987 (southern autumnal) equinox, as loss of the northern polar cap overlaps with re-freezing in the south, than near the 1861 and 2108 (northern autumnal) equinoxes.

light curves (Sicardy et al., 2006), but slightly exceeds the ~4×10^{18} CH_4/m^2 New Horizons Alice detection limit (Stern et al., 2017), suggesting that Charon's exosphere would have been borderline detectable had the spacecraft been present during the last northern spring exospheric maximum (Figure 2) in 1989.

Exospheric balance is achieved in the model over a Pluto orbit, with the cumulative number of arriving methane molecules, minus photo-destruction loss on the surface, balancing cumulative gravitational escape. However, the instantaneous escape and photolysis rates oscillate seasonally, tracking the exospheric and surface methane abundances as shown in Figure 2. Most of the methane escape occurs near the equinoxes coincident with the maximal exospheric gas abundance (Figure 2). The inverse of the average Jeans escape frequency of 2.7×10^{-6} s^{-1} yields the average methane in-flight lifetime of 4.2 (Earth) days (~242 hops on average). However, as the average CH_4 molecule spends ~99.99% percent of its life stuck to the surface, the actual lifetimes between arrival at Charon and loss are decades or centuries, with most molecules surviving several seasonal cycles before escaping. Our model indicates that, on average, ~10% of the methane arriving from Pluto is converted to surface photoproducts (~1.4×10^{23} CH_4/s average photo-destruction rate), with the remaining ~90% ultimately escaping Charon an average of ~155 years after arrival.

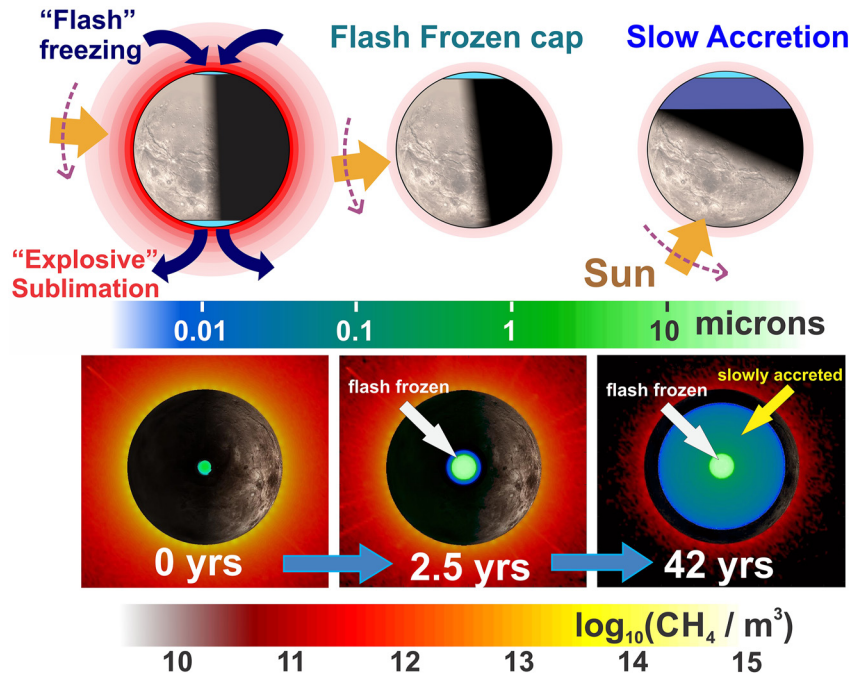

Figure 3. Top: Schematic showing how the "swap" of frozen methane between Charon's polar zones causes seasonal exospheric surges near Pluto system equinoxes (dashed arrow: insolation direction change with time). Bottom: Time lapse (north polar view) of the brief exospheric maximum near autumn equinox during which the initial ∼30 μm thick methane polar cap is flash frozen (snapshots 0 and 2.5 years post equinox), followed by exospheric collapse and decades long slow accretion of the more expansive sub-micron methane frost (+42 years). Red/yellow: equatorial exospheric CH_4 gas density cross section. Blue/green: Methane frost thickness. Simulation used a 10 J/m^2/K/s$^{0.5}$ thermal inertia and a 90° offset perihelion longitude.

A "flash-freezing" scenario, in which the autumn polar region is sufficiently cold (<∼30 K) to refreeze exospheric methane *during* an exospheric maximum, may occur in conditions of low thermal inertia (i.e., a porous regolith) and/or an enhanced CH_4 surface binding energy, or large scale topographic shadowing. Although topographical shadowing is not considered in our models, we note that Mordor Macula lies within a large scale depression (Schenk et al., 2018) that may remain in shadow beyond spring equinox, and therefore stay colder than the surrounding sunlit terrain. Methane molecules released from the spring hemisphere spend on average ∼2 (Earth) days executing random walk hops in the exosphere before refreezing to the opposite autumn hemisphere. Therefore, CH_4 jumps from pole to pole with each equinox, with most CH_4 molecules having only a few days per 248 year Pluto orbit in which to undergo gravitational escape. Most frozen methane is "flash frozen" near the equinoxes, as the exospheric density spikes over a roughly 4 year interval essentially instantaneous compared to a 248 year orbit.

Owing to the brevity of its formation, the flash frozen methane frost cap has a sharp edge (Figure 3) approximately coincident with the 30 K surface temperature isotherm circumscribing the autumn pole at equinox. As an example, we show in Figure 3 the time evolution of the polar frozen methane distribution near the autumnal equinox, assuming as in Figure 2 a 10 Jm^{-2}K^{-1}s$^{-0.5}$ surface thermal inertia (Grundy et al., 2016) and a 0.165 eV CH_4 binding energy. The predicted methane distribution exhibits a sharp edge at ∼80° latitude in this example, and the size of the frost cap appears similar to the extent of maximum red coloration observed in the Mordor Macula terrain (Figure 1).

A "slow accretion" phase in which methane continues to arrive from Pluto and condense gradually over the long polar night (Figure 3) occurs after the initial polar caps are flash frozen. Methane slowly accretes during the autumn-to-winter expansion and radiative cooling of the polar night zone, as colder isotherms of surface temperature expand from the pole to lower latitudes. The resulting "slowly accreted" distribution of condensed methane falls off more smoothly with latitude than the flash frozen polar cap over which it is deposited (Figures 3 and 4).

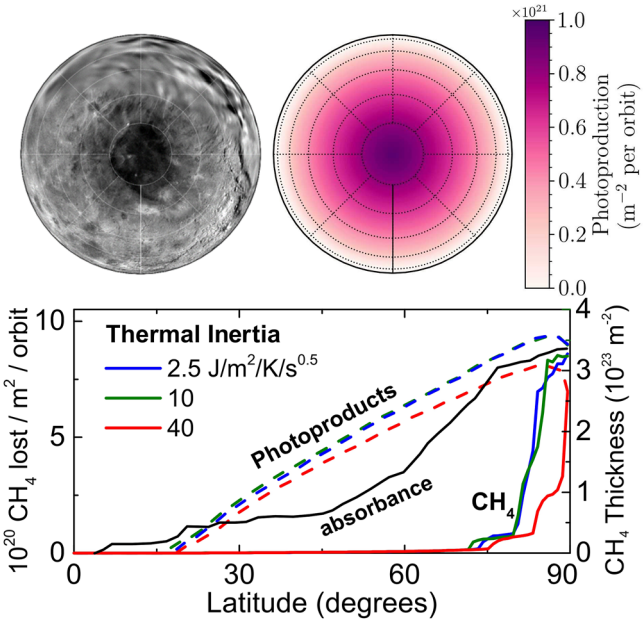

Figure 4. Top Right: Estimated cumulative photoproduct distribution synthesized over one Pluto orbit (units: CH_4 molecules photo-converted per m^2) from exospheric modeling with a 10 J/m^2/K/s$^{0.5}$ thermal inertia (15° latitude lines shown). Top Left: For comparison, Charon north polar composite map constructed from New Horizons MVIC + LORRI data (from the New Horizons Team (2017)). Bottom: Time-averaged frozen methane (solid; right axis) and photo-product (dashed; left axis) latitudinal distributions at different thermal inertias, compared to the surface longitudinally averaged optical absorbance 1-R where R is the reflectance from Grundy et al. (2016). We have averaged our results (top and bottom) over Pluto perihelion longitude to capture the estimated distributions over geologic time, and therefore the northern/southern distributions are identical. Methane peaks at high latitude owing to the flash frozen polar cap, but the polar cap shrinks at high thermal inertia (red). The methane column density far exceeds the amount $\eta_0 \sim 7 \times 10^{20}$ m^{-2} penetrable by Ly-α, and therefore photo-conversion is at all thermal inertias broadly distributed.

A "slow accretion only" scenario, in which the autumn polar zone is *not* sufficiently cold near equinox to freeze out exospheric methane, may also occur at higher thermal inertia (>∼10 J/m^2/K/s$^{0.5}$) and lower binding energy (<∼0.15 eV). In the slow accretion only scenario, there is a gap in time of a few years between the evaporation of the methane frost from the spring hemisphere and the commencement of methane accretion onto the autumn hemisphere. Methane desorbed from the spring hemisphere initially has nowhere to re-freeze, and therefore a slightly larger fraction of methane arriving at Charon is lost to gravitational escape on average in the slow accretion only scenario, than in the flash freezing scenario (92 vs. 90%, respectively).

Pluto's highly eccentric heliocentric orbit, and its 2.8 MYr precession cycle (Dobrovolskis et al., 1997), also influence Charon's exosphere and surface photoproduct distribution. Presently, Pluto's semi-major axis is almost co-aligned with the equinoxes, with perihelion (aphelion) preceding the southern (northern) autumnal equinoxes by only 2 years. Owing to the present-day factor 1.66 difference in heliocentric distances between the equinoxes, Charon's modeled surface temperatures are a few Kelvin colder at northern autumn as the exosphere surges off the south, than in southern autumn when the exosphere comes off the north. In this circumstance, a flash-frozen exosphere forms a more expansive frost cap over the north than the south, since the north is colder during polar sunset than is the south during its sunset. The predicted flash frozen methane distribution therefore extends ∼5° further from the north pole than from the south pole; that is, at Pluto's current longitude of perihelion more methane is being frozen in Charon's north.

Over time the precession of the equinoxes changes this situation. At longitudes of perihelion offset +/−90° from present day, which last occurred ∼700 kYr ago, the equinoxes are nearly co-aligned to Pluto's semi-*minor* axis and approximately equidistant from the Sun. For these perihelion longitudes Charon's north and south poles are at similar temperatures during the polar sunsets, and Charon's northern and southern frozen methane distributions are predicted to be similar. For a 180° perihelion offset, which last occurred ∼1.4 MYr ago, the situation is opposite to present day, with perihelion coincident with the northern (rather than southern) autumnal equinox, and more photoproducts produced in Charon's south.

The predicted photoproduct distribution is much broader than for methane (Figure 4, bottom) because the methane polar frost is too thick for the Ly-α light to penetrate. Ly-α light's penetration depth in solid methane is only ∼35 nm (Martonchik and Orton, 1994), much less than the polar cap's several tens of microns initial thickness after a flash freezing event (Figure 3). As a result, the predicted photoproduct distribution exhibits a smooth dependence on latitude that tracks approximately the duration of the winter frost at that latitude. After the initial polar cap is rapidly flash frozen, more CH_4 frost continuously freezes onto the polar night zone in the slow accretion phase (Figure 3), growing an estimated ∼300 nm over the $1/\sigma_d F_{Ly\alpha} \sim 100$ years photo-conversion time; that is, an order of magnitude faster than the topmost ∼35 nm is photo-converted. These CH_4 accretion rates on the order ∼10^{12} m^{-2}s^{-1}, and surging briefly near the poles as high as ∼3×10^{16} m^{-2}s^{-1} during the equinoctial flash-freezing episodes, are ∼4–30,000 times the 3.5×10^{11} m^{-2}s^{-1} Ly-α flux. At such high (>>1) ratios of CH_4 accretion to Ly-α flux the photoproduct concentration in Charon's methane frost is highly diluted (0.001%–15%), depending on latitude, time, and depth in the frost layer. For this reason we estimate that, after averaging the precession effect and assuming a 10 J/m^2/K/s$^{0.5}$ thermal inertia (Grundy et al., 2016), only ∼10% of the methane arriving from Pluto is converted to surface photoproducts over geologic time. Our calculation is about half the 21% conversion estimated by Grundy et al. (2016), owing to the seasonal flash-freezing effect considered here, and resulting rapid deposition of optically thick methane frost at the polar zone.

Ethane, according to experiment (Lo et al., 2015; Raut et al., 2022), constitutes a large (>∼60%) proportion of Charon's photolytic material owing to the dilution effect, as rapid methane accretion and burial below the optical depth hinders photo-processing of new C_2H_6 molecules into higher-order hydrocarbons. Ethane will remain stuck to the surface for a decade or more after the spring methane sublimation, undergoing solar wind processing into higher-order refractory hydrocarbons before itself being volatilized into the exosphere near Charon's ∼60 K maximum surface temperature. How photolytic ethane contributes to Charon's exosphere, and to the red material, for example, by re-distributing itself seasonally on the dayside surface under exposure and radiolysis by the solar wind, is a question yet to be answered. A more complete understanding will likely require multi-species exospheric modeling including both methane and ethane, while accounting for the effects of both Ly-α photolysis and solar wind.

Micrometeoroid turnover mixes refractory hydrocarbons downward as they are produced, and hence the regolith's refractory abundance represents the cumulative average production over many precession cycles. We therefore show precession-averaged frozen methane and photoproduct distributions in Figure 4, obtained by performing exospheric simulations at several longitudes of perihelion. As an approximation, we have neglected other minor aspects of the precession; specifically the obliquity and eccentricity cycles between 104 and 127° and 0.22 and 0.27 (Dobrovolskis et al., 1997). We find as expected that the precession averaged polar methane and photoproduct distributions are identical in both Charon hemispheres.

The age of the red material seen by MVIC depends on the competition of surface refractory production with turnover of regolith already infused with older refractories. Using as an analog to Charon the expression $x = 2 \times 10^{-6} \times t^{0.61}$ of Costello et al. (2018) for lunar regolith turnover depth x versus time t, and assuming a regolith grain size $x_1 = 50$ μm for the optical scattering depth (Protopapa et al., 2021) observable by MVIC, we calculate a turnover time $t_1 = 134$ years. This contributes a negligible $t_1 x_2 / t_2 x_1 = 0.3\%$ to the refractory concentration already in the surface regolith produced, for example, just over the last $t_2 = 1$ billion years (357 precession cycles) if distributed down to the mixing depth $x_2 \sim 1$ m for that time period. Impact gardening rates for the outer solar system are uncertain, but the takeaway is that the red material visible to the MVIC camera probably mixes rapidly enough from beneath the optical scattering depth that it is likely to be old; the product many Charon seasons and precession cycles.

4. Conclusions

The proposition that Charon's entire exosphere may undergo regular ultra-short lived spikes of high gas density constitutes, if correct, an extraordinary discovery of the New Horizons mission. These seasonal exospheric dynamics, together with the action of Ly-α photolysis as posited by Grundy et al. (2016), appear to provide at least a partial explanation for Charon's red material distribution. Equally remarkable is that methane frost may be bi-annually flash frozen during exospheric spikes, as frozen methane is swapped from pole to pole, forming flash frozen polar caps tens of microns in thickness and of similar extent to Charon's red spot. However, the insufficiency of Ly-α light's penetration depth to fully process this initial autumnal polar frost paints a more complicated picture, with most methane photoproducts produced over a broader latitudinal area (Figure 4) as additional methane slowly freezes and is photolyzed over the long polar night. Frozen ethane, the primary surface photoproduct, may stick to Charon's polar surface in daylight long enough for radiolysis by the solar wind before itself becoming volatilized into the exosphere. These discoveries, and the fresh questions raised by them, are a vivid exposition of the combined power of spacecraft data and modeling to elucidate the physics of a planetary system, and they cast new light on the understanding of seasonal methane photolysis and radiolysis at Charon (Grundy et al., 2016) by revealing the probable role of Charon's extreme exospheric dynamics in shaping its red spot.

Data Availability Statement

Data and models associated with this manuscript are available on the Zenodo repository at https://doi.org/10.5281/zenodo.6423945.

Acknowledgments
Work supported by the NASA New Frontiers Data Analysis Program Grant No. 80NSSC18K1391. We thank CLASSE team members Michael Poston, Josh Brody, and Preston Karnes for helpful discussions on the science and manuscript.

References

Armstrong, G. T., Brickwedde, F., & Scott, R. (1955). Vapor pressures of the methanes. *Journal of Research of the National Bureau of Standards*, *55*(1), 39–52. https://doi.org/10.6028/jres.055.005

Bagenal, F., Horányi, M., McComas, D. J., McNutt, R. L., Jr., Elliott, H. A., Hill, M. E., et al. (2016). Pluto's interaction with its space environment: Solar wind, energetic particles, and dust. *Science*, *351*, 6279.

Cheng, A. F., Weaver, H. A., Conard, S. J., Morgan, M. F., Barnouin-Jha, O., Boldt, J. D., et al. (2008). Long-range reconnaissance imager on new Horizons. *Space Science Reviews*, *140*, 189–215. https://doi.org/10.1007/978-0-387-89518-5_9

Costello, E. S., Ghent, R. R., & Lucey, P. G. (2018). The mixing of lunar regolith: Vital updates to a canonical model. *Icarus*, *314*, 327–344. https://doi.org/10.1016/j.icarus.2018.05.023

Dobrovolskis, A. R., Peale, S. J., & Harris, A. W. (1997). In A. Stern, & D. J. Tholen (Eds.), *Dynamics of the Pluto-Charon Binary Pluto and Charon*. University of Arizona Press.

Gladstone, G. R., Pryor, W. R., & Stern, A. S. (2015). Lya@Pluto. *Icarus*, *246*, 279

Grava, C., Chaufray, J. Y., Retherford, K. D., Gladstone, G. R., Greathouse, T. K., Hurley, D. M., et al. (2015). Lunar exospheric argon modeling. *Icarus*, *255*, 135–147. https://doi.org/10.1016/j.icarus.2014.09.029

Grundy, W. M., Cruikshank, D. P., Gladstone, G. R., Howett, C. J. A., Lauer, T. R., Spencer, J. R., et al. (2016). The formation of Charon's red poles from seasonally cold-trapped volatiles. *Nature*, *539*(7627), 65–68. https://doi.org/10.1038/nature19340

Hoey, W. A., Yeoh, S. K., Trafton, L. M., Goldstein, D. B., & Varghese, P. L. (2017). Rarefied gas dynamic simulation of transfer and escape in the Pluto–Charon system. *Icarus*, *287*, 87–102. https://doi.org/10.1016/j.icarus.2016.12.010

Huebner, W. F., Keady, J. J., & Lyon, S. P. (1992). Solar photo rates for planetary atmospheres and atmospheric pollutants. *Astrophysics and Space Science*, 195–289. https://doi.org/10.1007/978-94-017-3023-5_1

Lo, J.-I., Lin, M.-Y., Peng, C.-Y., Chou, S.-L., Lu, C.-H., Cheng, M.-B., & Ogilvie, J.-F. (2015). Far-ultraviolet photolysis of solid methane. *Monthly Notices of the Royal Astronomical Society*, *451*(1), 159–166. https://doi.org/10.1093/mnras/stv935

Martonchik, J. V., & Orton, G. S. (1994). Optical constants of liquid and solid methane. *Applied Optics*, *33*(36), 8306. https://doi.org/10.1364/ao.33.008306

Protopapa, S., Cook, J. C., Grundy, W. M., Cruikshank, D. P., Dalle Ore, C. M., & Beyer, R. A. (2021). Surface composition of Charon. In *Pluto system after new horizons*, edited, (p. 435). University of Arizona Press.

Raut, U., Teolis, B. D., Kammer, J. A., Gimar, C. J., Brody, J. S., Gladstone, G. R., et al. (2022). Role of photolysis in the origin of Charon's red polar albedo. *53rd Lunar & planetary Science Conference*, LPI Contribution No. 2678, id. 1580

Reuter, D. C., Stern, S. A., Scherrer, J., Jennings, D. E., Baer, J. W., Hanley, J., et al. (2008). Ralph: A visible/infrared imager for the new horizons pluto/Kuiper belt mission. *Space Science Reviews*, *140*(1), 129–154. https://doi.org/10.1007/s11214-008-9375-7

Schenk, P. M., Beyer, R. A., McKinnon, W. B., Moore, J. M., Spencer, J. R., White, O. L., et al. (2018). Breaking up is hard to do: Global cartography and topography of Pluto's mid-sized icy Moon Charon from new horizons. *Icarus*, *315*, 124–145. https://doi.org/10.1016/j.icarus.2018.06.010

Sicardy, B., Bellucci, A., Gendron, E., Lacombe, F., Lacour, S., Lecacheux, J., et al. (2006). Charon's size and an upper limit on its atmosphere from a stellar occultation. *Nature*, *439*(7072), 52–54. https://doi.org/10.1038/nature04351

Stern, S. A., Kammer, J., Gladstone, G., Steffl, A., Cheng, A., Young, L., et al. (2017). New horizons constraints on Charon's present day atmosphere. *Icarus*, *287*, 124–130. https://doi.org/10.1016/j.icarus.2016.09.019

Teolis, B. D., & Waite, J. H. (2016). Dione and Rhea seasonal exospheres revealed by Cassini CAPS and INMS. *Icarus*, *272*, 277–289. https://doi.org/10.1016/j.icarus.2016.02.031

The New Horizons Team. (2017). *LORRI MVIC global mosaic 300m v1*. JHUAPL. Retrieved from https://astrogeology.usgs.gov/search/map/Charon/NewHorizons/Charon_NewHorizons_Global_Mosaic_300m_Jul2017

Tucker, O. J., Johnson, R. E., & Young, L. A. (2015). Gas transfer in the Pluto-Charon system: A Charon atmosphere. *Icarus*, *246*, 291–297. https://doi.org/10.1016/j.icarus.2014.05.002